Anisotropic lattice dynamics and intermediate-phase magnetism in delafossite $CuFeO_2$

B. Klobes* and M. Herlitschke†
Jülich Centre for Neutron Science JCNS and Peter Grünberg Institute PGI, JARA-FIT, Forschungszentrum Jülich GmbH, 52425 Jülich, Germany

K. Z. Rushchanskii
Peter Grünberg Institut, Quanten-Theorie der Materialien, Forschungszentrum Jülich and JARA, 52425 Jülich, Germany

H.-C. Wille
FS-PE, Deutsches Elektronen-Synchrotron (DESY), 22607 Hamburg, Germany

T. T. A. Lummen‡ and P. H. M. van Loosdrecht§
Zernike Institute for Advanced Materials, University of Groningen, Nijenborgh 4, 9747 AG Groningen, The Netherlands

A. A. Nugroho
Faculty of Mathematics and Natural Sciences, Institut Teknologi Bandung, Jl. Ganesha 10, 40132 Bandung, Indonesia

R. P. Hermann‖
Jülich Centre for Neutron Science JCNS and Peter Grünberg Institute PGI, JARA-FIT, Forschungszentrum Jülich GmbH, 52425 Jülich, Germany and Faculté des Sciences, Université de Liège, 4000 Liège, Belgium

(Received 23 May 2015; published 20 July 2015)

Hyperfine interactions and Fe-specific lattice dynamics in $CuFeO_2$ were investigated by nuclear resonance scattering methods and compared to *ab initio* lattice dynamics calculations. Using nuclear forward scattering the collinear spin structure at temperatures below about 11 K could be confirmed, whereas the nuclear forward scattering results in the intermediate temperature range between about 11 K and 14 K are incompatible with the assumption of a sinusoidal distribution of spins parallel to the c axis of $CuFeO_2$. The critical behavior of the average hyperfine field at the phase transition at about 14 K further supports a three-dimensional model for the magnetism in this compound. Moreover, using nuclear inelastic scattering by the ^{57}Fe Mössbauer resonance, Fe-specific lattice dynamics are found to be strongly anisotropic with stiffer bonds in the ab plane of the crystal. The powder averaged, Fe partial density of phonon states can be well modeled using *ab initio* calculations and low-energy phonons are found to deviate from classical Debye-like behavior, indicating spin-phonon coupling in this compound. Besides, the theoretical phonon spectrum exhibits typical characteristics for delafossite-type material.

DOI: 10.1103/PhysRevB.92.014304 PACS number(s): 76.80.+y, 75.40.Cx, 63.20.dk

I. INTRODUCTION

Delafossite $CuFeO_2$ archetypally embodies several aspects of modern condensed-matter physics research such as complex magnetism, multiferroicity, and the quest for new applications. The magnetic phase diagram of $CuFeO_2$ proves to be particularly rich with various magnetic phases at low temperatures, high magnetic fields [1–4], and high pressures [5,6]. Ferroelectricity [7] in $CuFeO_2$ and its connection to the magnetic order is the subject of ongoing studies [8,9]. From an application-oriented perspective, $CuFeO_2$ and other delafossite-type oxides are investigated as potential thermoelectric materials [10,11].

At room temperature, $CuFeO_2$ has space group $R\bar{3}m$ with $a = b = 3.035$ Å and $c = 17.166$ Å in the hexagonal setting [12] (see inset to Fig. 1) and can be visualized as a sequence of (stacked) hexagonal Cu, O, Fe, and O layers along the c axis. Each layer of magnetic Fe^{3+} ions ($^6S_{5/2}$ ground state) constitutes a two-dimensional, triangular lattice, which in combination with antiferromagnetic interactions represents a classical case of geometric frustration. Despite its electronic configuration, which *prima facie* suggests isotropic antiferromagnetic exchange interactions, $CuFeO_2$ adopts a collinear, Ising-like magnetic structure at low temperatures below 11 K. In zero magnetic field, two structural [13,14] and magnetic transitions are observed at $T_{N1} \approx 14$ K and $T_{N2} \approx 11$ K. Structurally, $CuFeO_2$ transforms to space group $C2/m$ at T_{N1} and to lower monoclinic symmetry at T_{N2}. Above T_{N1}, $CuFeO_2$ is paramagnetic (PM), whereas the magnetic structure in the intermediate temperature phase (ITP), i.e., $T_{N2} < T < T_{N1}$, is usually considered a

*b.klobes@fz-juelich.de
†Present address: FS-PE, Deutsches Elektronen-Synchrotron (DESY), 22607 Hamburg, Germany.
‡Present address: Laboratory for Ultrafast Microscopy and Electron Scattering, ICMP, École Polytechnique Fédérale de Lausanne, Station 6, 1015 Lausanne, Switzerland.
§Present address: II. Physikalisches Institut, University of Cologne, Zülpicher Strasse 77, 50937 Cologne, Germany.
‖Present address: Materials Science and Technology Division, Oak Ridge National Laboratory, Oak Ridge, Tennessee 37831, USA.

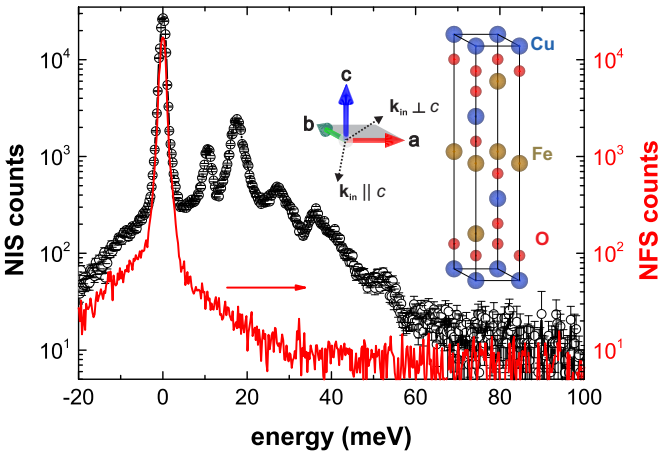

FIG. 1. (Color online) Representative NIS and time-integrated NFS spectra of $CuFeO_2$ obtained at 8.5 K. The instrumental resolution obtained in the NFS channel exhibits a full width at half maximum of 1.2 meV. Additionally, the room-temperature crystal structure of $CuFeO_2$ and a sketch of the two measurement configurations are shown. Note the tilt angles in both cases.

quasi-long-range ordered, sinusoidally amplitude modulated, incommensurate structure with a temperature-dependent propagation vector [15] and a potential, residual paramagnetic contribution [16]. At T_{N2}, $CuFeO_2$ reaches its collinear four-sublattice magnetic ground state (4SL) with spins aligned (anti)parallel along the c axis adopting an up-up-down-down order [17]. The stabilization of the Ising-like 4SL structure can be attributed to a low-temperature structural distortion resulting in unequal nearest-neighbor exchange interactions [13,14,18,19]. Alternatively, the distortion may yield a weak magnetic anisotropy [20], which in combination with a rather strong spin-phonon coupling can give rise to the Ising-like behavior [2,3,21]. The relevance of the coupling between vibrational properties and magnetic degrees of freedom for both zero field phase transitions in $CuFeO_2$ was also pointed out in Refs. [22,23]. In particular, the pseudoproper ferroelastic phase transition at T_{N1} was concluded to drive the simultaneous magnetic transition, which is accompanied by a softening of elastic constants [22]. This immediately raises the question as to whether magnetoelastic coupling in $CuFeO_2$ is mainly related to acoustical or optical phonons or whether it is reflected in the total lattice dynamics. Besides, the layered structure of $CuFeO_2$ suggests a pronounced vibrational anisotropy, which is yet to be confirmed. Furthermore, in contrast to the magnetic ground state at zero magnetic field and magnetic phases at high fields, which generally exhibit rather well defined spin structures [3,4], the magnetic ITP has received considerably less attention and is not yet convincingly described.

Here we report a nuclear resonance scattering study of the magnetic structure and Fe-specific lattice dynamics in all three phases at zero magnetic field. Using nuclear forward scattering the temperature-dependent evolution of the magnetic structure is followed and Fe partial densities of phonon states are derived from nuclear inelastic scattering data, which provides direct access to the vibrational properties of the magnetic sublattice via the ^{57}Fe Mössbauer resonance. Lattice dynamics are also investigated using theoretical calculations.

II. EXPERIMENTAL AND THEORETICAL DETAILS

Nuclear resonance scattering [24] (NRS) experiments were carried out at the nuclear resonance beamline [25] P01 of the synchrotron radiation source PETRA III, DESY. Using a high-resolution monochromator with an energy resolution of 1.2 meV [26] (full width at half maximum) at the 14.4125-keV Mössbauer resonance of ^{57}Fe, the Fe-specific density of phonon states (DPS) and hyperfine interactions were accessed. Nuclear inelastic scattering (NIS) spectra (a representative NIS spectrum is shown in Fig. 1) were analyzed employing the Fourier-log decomposition as implemented in the software DOS [27], in order to extract Fe partial DPS, and time-resolved nuclear forward scattering (NFS) spectra were analyzed using the software MOTIF [28], in order to model hyperfine interactions.

A single crystal of $CuFeO_2$ was grown by the floating zone technique as outlined in Ref. [29] in a four-mirror furnace. In order to increase the measurement signal, a small ^{57}Fe-enriched section was introduced into the large polycrystalline template before growing the crystal in a floating zone furnace. The enriched crystal section was located by nuclear fluorescence with an enrichment of about 90% [4]. The single crystal was oriented to within 2°, polished to a thickness of 48 μm, glued onto a 155-μm diamond substrate, and attached to a closed-cycle He cryostat near a thermocouple for NRS measurements.

The investigation of a single-crystal sample using NIS does *not* yield the total (Fe partial) DPS, $g(E)$, because the probability of the NIS process depends on the projection of the wave vector of the incident beam, $\mathbf{k}_{\mathrm{in}}$, onto the polarization vector $\mathbf{e}_j(\mathbf{q})$ of the nuclear resonant atomic vibrations for phonon branch j with phonon wave vector $\mathbf{q}$. Instead, a projected DPS [30] can be obtained,

$$g(E,\mathbf{s}) = \frac{V_0}{(8\pi^3)} \sum_j \int d\mathbf{q}\, \delta[E - h\omega_j(\mathbf{q})] |\mathbf{s}\cdot\mathbf{e}_j(\mathbf{q})|^2, \quad (1)$$

where V_0 is the volume of the unit cell and $\mathbf{s} = \mathbf{k_{in}}/k_{\mathrm{in}}$. In order to account for potential vibrational anisotropy, the $CuFeO_2$ single crystal was investigated in two different configurations, i.e., with $\mathbf{k_{in}} \parallel c$ and $\mathbf{k_{in}} \perp c$. These measurement settings thus specifically probe vibrations with polarization or atomic displacements parallel to the c axis and within the ab plane [31], respectively. As only projected densities of phonon states were measured for this study, the variable $\mathbf{s}$ will be dropped and all DPS will be referenced by $g(E)$ below.

The exact orientation of the crystal was determined by means of NFS as described in Sec. III A. Usually, the detailed-balance principle of phonon creation and annihilation in an NIS spectrum is used in order to determine the sample temperature. However, low statistics at low temperatures on the phonon annihilation side of NIS spectra combined with the left shoulder of the instrumental resolution function (see Fig. 1) prevent a reliable temperature determination by the latter principle. Instead, the NFS data obtained in the 4SL and PM phase regions were used as temperature indicators (see below).

Structural properties of $CuFeO_2$ were theoretically investigated using the Vienna Ab-initio Simulation Package [32–34] (VASP). We use projector-augmented wave pseudopotentials

[35] with the valence-electron configurations $3d^{10}4s^1$ for Cu, $3p^6 3d^7 4s^1$ for Fe, and $2s^2 2p^4$ for O. Spin-polarized local density approximation [36] (LDA) was used to account for exchange and correlation energy. Due to strong correlation effects on Fe d electrons, the LDA + U approach [37] with on-site Coulomb parameter $U = 5$ eV and Hund's exchange parameter $J = 1$ eV was employed, whereas spin-orbit effects were neglected. A kinetic energy cutoff of 700 eV for the determination of the plane-wave basis and a 8×8×8 Γ-centered Monkhorst-Pack k-point mesh [38] for Brillouin zone integration were used. Structural parameters of the unit cell were obtained by minimization of the Hellman-Feynman forces to values less than 1 meV per Å. In all calculations, $R\bar{3}m$ (No. 166) structure in the high-symmetry configuration and ferromagnetically aligned Fe magnetic moments (for calculational simplicity) were used. Theoretically obtained lattice parameters, $a = 2.976$ Å and $c = 17.0$ Å, are in reasonable agreement with experimental room-temperature values [11,12], $a_{\mathrm{exp}} \approx 3.035$ Å and $c_{\mathrm{exp}} \approx 17.167$ Å, as an underestimation by 1.9% for a and 1.0% for c parameter is typical for LDA. Moreover, the position of oxygen, $z = 0.1058$, is in excellent agreement with experimental data [11,39].

Phonon spectra were calculated using the force-constant method [40] as implemented in the PHON code [41]. Hellman-Feynman forces for atomic displacements of 0.04 Å from their equilibrium positions are calculated in a 4×4×4 supercell. The Γ-centered k-point mesh was reduced to 2×2×2 for supercell calculations. For phonons at arbitrary q points, the dynamical matrix is obtained by Fourier transformation of the *ab initio* force constants as calculated for the Γ point and for the Brillouin zone boundaries. q-point phonon mode wave numbers and corresponding atomic displacement patterns were obtained as eigenvalues and eigenvectors of the corresponding dynamical matrix. The DPS was calculated in a 30×30×30 q-point mesh and additionally convoluted with a Gaussian function in order to account for experimental resolution.

III. RESULTS AND DISCUSSION

A. Hyperfine interactions by NFS

Time-resolved NFS measurements at different temperatures obtained with $\mathbf{k_{in}}$ almost parallel to the c axis of the $CuFeO_2$ sample are shown in Fig. 2. The NFS patterns at high temperatures, i.e., at 15 K and 20 K, are archetypal examples for nuclear level splittings completely determined by an electric field gradient (EFG). Accordingly, $CuFeO_2$ is in its paramagnetic state and these two spectra allow for deriving the exact crystal orientation with respect to the incident beam by means of the EFG direction, which is known to be parallel to the c axis [42] of $CuFeO_2$. The quadrupole splitting [43] resulting from the existence of the EFG was determined to be $6.7(2)\Gamma_0$ or 0.65(2) mm/s in good agreement with conventional Mössbauer spectroscopy results [42]. The quadrupole splitting was assumed to be constant at all temperatures below 15 K, in order to reduce the number of fit parameters. At temperatures below or equal to 11.5 K, the NFS data can be modeled assuming two equally occupied nuclear sites with hyperfine fields of the same absolute value but antiparallel alignment along c. As in the case of NFS different Fe sites are exclusively distinguishable from each other by differing hyperfine interactions [44], the latter cases clearly represent the low-temperature, collinear antiferromagnetic case of the 4SL phase. The mean absolute value of the hyperfine field, $|\overline{B_{hf}}|$, shown in the inset to Fig. 4 reasonably agrees with Mössbauer spectroscopy results at low temperatures [42]. Beside the verification of the (known) magnetic structure below 11.5 K and above 15 K, the consistency of the present results with published transition temperatures shows that the temperature calibration and determination is accurate with a temperature offset of 0.5 K at most. Moreover, the angle between the c axis and $\mathbf{k_{in}}$ in the parallel setting could be determined to be 10° and the angle between $\mathbf{k_{in}}$ and the ab plane was 25° in the perpendicular setting (the NFS data measured in the latter setting at $T = 8.5$ K, 11.5 K, and 20 K is not shown here).

In contrast to the PM and 4SL phases, the NFS data in the intermediate temperature region is characterized by less defined beating patterns, indicating increased complexity. As NFS is based on a nuclear exciton involving all resonant nuclei in the sample, the technique is insensitive to the propagation vector and, thus, should be solely characterized by the sinusoidal distribution of hyperfine fields. Taking into account the determined crystal orientation and quadrupole splitting and assuming a sinusoidal distribution [45] of $|\overline{B_{hf}}|$ with different maximum values, the expected NFS signal was calculated and is shown in Fig. 3.

Comparing these simulations with the experimental NFS data in the ITP region (see Fig. 2), it is rather clear that the experimental NFS signal cannot be modeled with a sinusoidal distribution of hyperfine fields. The assumption of paramagnetism for 1/5 of the nuclear sites [16], which is also shown in Fig. 3 for the 40 T case, also seems unlikely comparing experimental NFS data and the corresponding simulation. Moreover, it should be noted that conventional energy domain Mössbauer spectroscopy results [46] do not show any paramagnetic contribution in the intermediate temperature range.

The problem of fitting the NFS data in the ITP region was approached on a purely phenomenological basis instead, using different nuclear sites with relative contribution and hyperfine field as free parameters. The results of this procedure, i.e., the relative contribution of different nuclear sites and their respective hyperfine fields, are depicted in Fig. 4.

In general, the hyperfine field at the different nuclear sites continuously increases with decreasing temperature. In contrast to the 4SL phase, the ratio of nuclear sites with B_{hf} aligned parallel and antiparallel to the c axis is not 1 and the change of the hyperfine field also differs with respect to the two alignment directions. These results may not microscopically represent the magnetic structure of $CuFeO_2$ in the ITP, but, in any case, the notion of a sinusoidal distribution of hyperfine fields and spins is seriously challenged.

In principle, the hyperfine field $|\overline{B_{hf}}|$ (see inset to Fig. 4) also allows for inspecting the critical behavior [47] at T_{N1} as $|\overline{B_{hf}}| \propto (1 - T/T_{N1})^{\beta}$, where β is the critical exponent. Due to the rather small number of data points, β was fixed to 0.125 and 0.34, representing two- and three-dimensional models [47,48], respectively. In both cases, T_{N1} was determined to be about 14.6(2) K. However, using $\beta = 0.125$, no reasonable

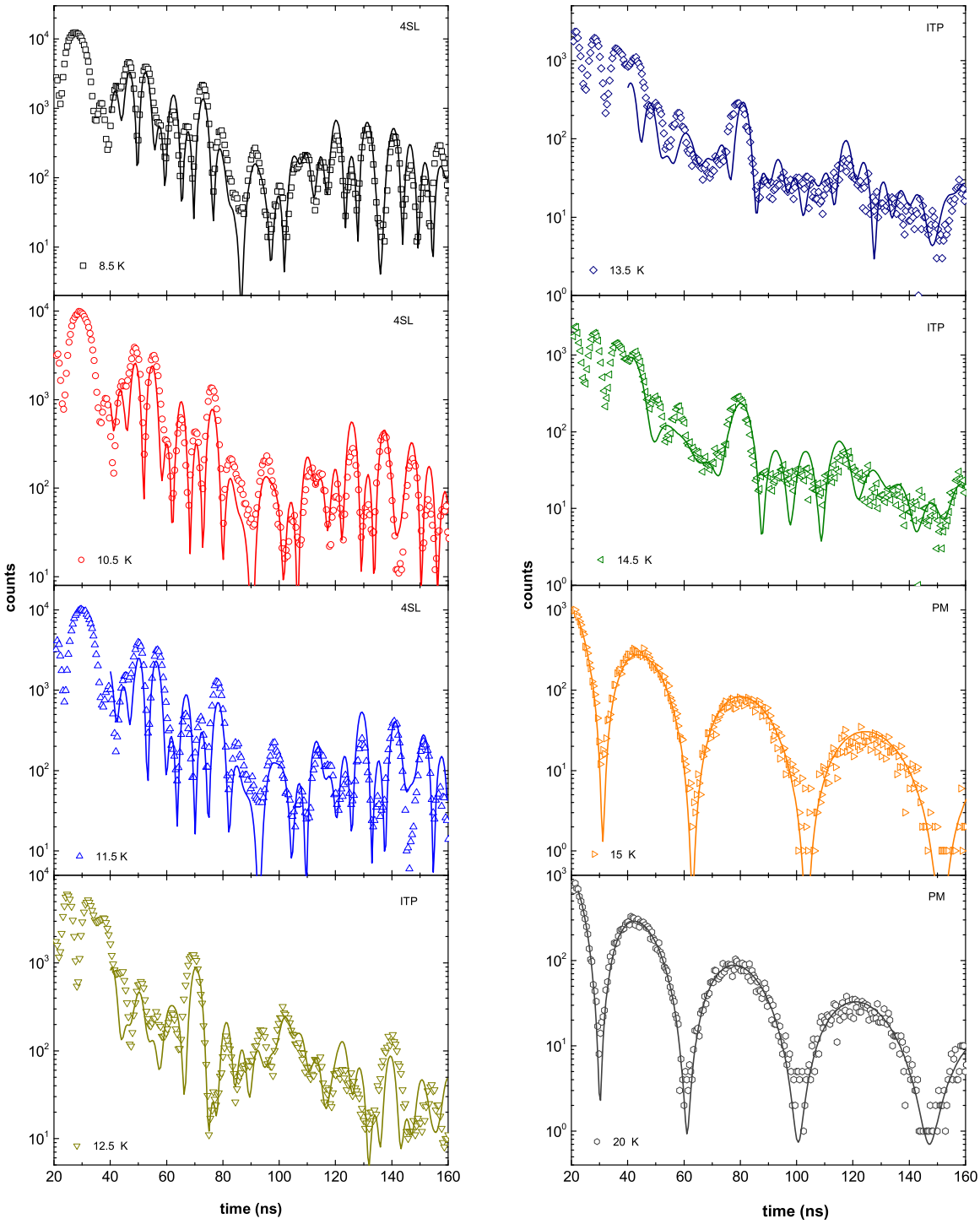

FIG. 2. (Color online) Time-resolved NFS spectra of $CuFeO_2$ measured at various temperatures with c axis almost parallel to the incident beam. Corresponding fits are shown as solid lines.

fit could be obtained and, thus, only the fit using $\beta = 0.34$ is shown in the inset to Fig. 4. The superior agreement with the fit using $\beta = 0.34$ supports a three-dimensional model for magnetism [47,48] in $CuFeO_2$, which was also supported in Ref. [49] and is in line with Ref. [50] observing a Cu-mediated interlayer interaction. However, it is not possible to distinguish between the Heisenberg, Ising, or XY model [48] on the basis of the presented data. Notably, similar results concerning the critical exponent β, i.e., the three-dimensional nature of magnetism, were reported [51] for isostructural $AgFeO_2$ recently.

B. Fe-specific lattice dynamics: NIS

NIS measurements were taken at 20 K, 13.5 K, and 8.5 K for the ($\mathbf{k_{in}} \parallel c$) and at 20 K and 8.5 K for the ($\mathbf{k_{in}} \perp c$) setting. As

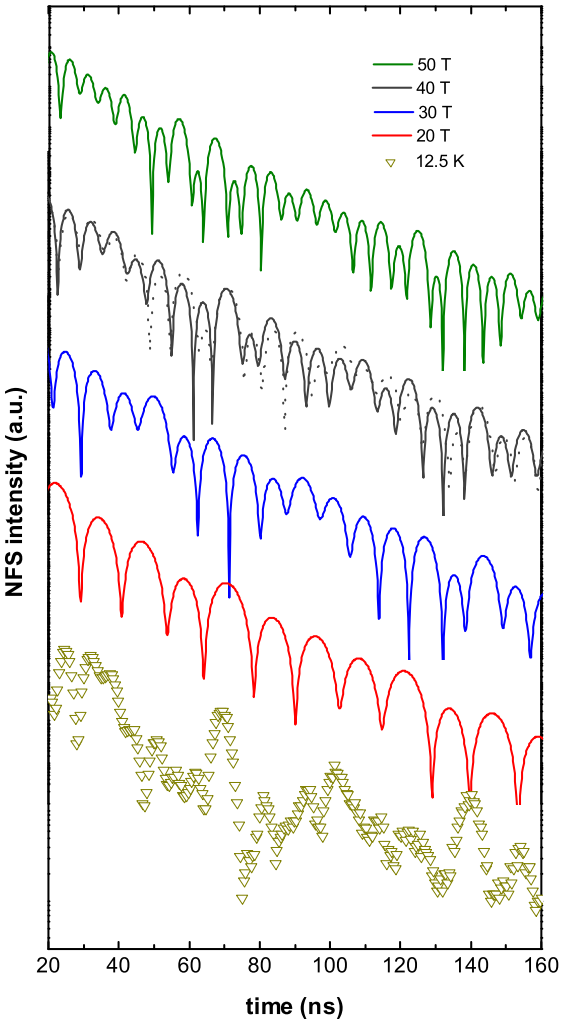

FIG. 3. (Color online) Simulated NFS spectra assuming sinusoidally modulated spins oriented along the c axis. Except for the hyperfine magnetic field, all other parameters, i.e., crystal orientation with respect to the incident beam and quadrupole splitting value, were the same as those used to fit the experimental data as shown in Fig. 2. The dotted line represents the impact of assuming 1/5 of the spins to be paramagnetic and 4/5 to exhibit a sinusoidal hyperfine field distribution with 40 T maximum. Experimental data measured at 12.5 K is shown for comparison.

no significant difference between the DPS derived at different temperatures could be detected, the Fe-specific DPS projected onto the c axis and onto the ab plane are shown exclusively for 20 K in the top part of Fig. 5. Because data close to zero energy transfer, in particular for energies below 4 meV, are strongly affected by the elastic line and the details of the subtraction procedure, this low-energy part is omitted. A pronounced vibrational anisotropy between different phonon polarizations is obvious. Optical phonons polarized within the ab plane have significantly more spectral weight and occur at higher energies as compared to phonons polarized along the c axis. Notably, the DPS representing the latter polarization direction is mainly characterized by two sharp van Hove singularities at about 10 and 18 meV and two further, rather broad peaks at about 28 and 38 meV.

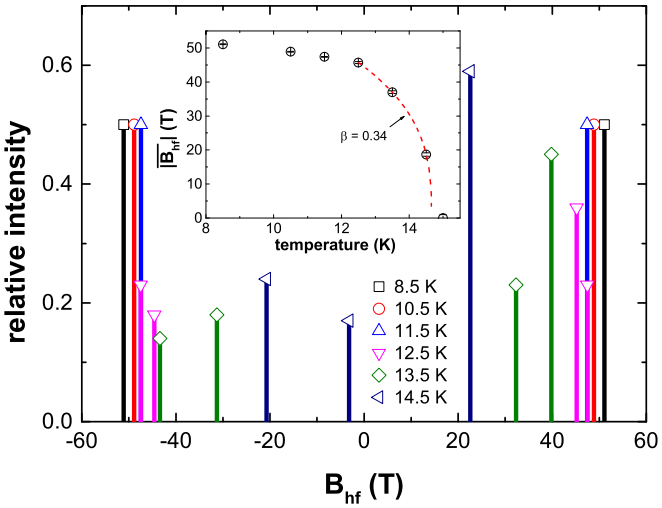

FIG. 4. (Color online) Relative contribution of nuclear sites with different hyperfine fields as obtained by fitting the NFS data shown in Fig. 2. The sign of B_{hf} represents parallel and antiparallel alignment along c or vice versa. The mean absolute value of the hyperfine field at decreasing temperature is shown in the inset. The dashed line represents critical behavior with $\beta \approx 0.34$ (see text).

Taking into account the projectional character of the DPS with respect to the measurement configuration as well as the directional isotropy around Fe in the ab plane, it is possible to reconstruct the total (powder average) DPS from the projected DPS taking into account the tilt angles for both measurement configurations. The total powder average Fe-specific DPS in $CuFeO_2$ is shown in the bottom half of Fig. 5 and compared to *ab initio* calculations, which show a good agreement and are discussed in more detail below. Raman modes are also shown in Fig. 5, but the atomic displacements of Fe for the two observed Raman modes with E_g and A_{1g} symmetry vanish [52]. Thus, they cannot be observed using NIS.

Based on $g(E)$ the Fe-specific mean force constant $\overline{F}$, the vibrational entropy $S_{\rm vib}$, the internal energy $E_{\rm int}$, and the Lamb-Mössbauer factor $f_{\rm LM}$ quantifying the recoilless absorption probability can be calculated [27],

$$\overline{F} = \frac{m}{\hbar^2}\int_0^\infty g(E)E^2 dE, \tag{2}$$

$$S_{\rm vib} = 3k_B\int_0^\infty g(E)\{[n(E,T)+1]\ln[n(E,T)+1] - n(E,T)\ln[n(E,T)]\}dE, \tag{3}$$

$$E_{\rm int} = \frac{3}{2}\int_0^\infty g(E)\,E\coth\left(\frac{E}{2k_BT}\right)dE, \tag{4}$$

$$f_{\rm LM} = \exp\left[-E_R\int_0^\infty g(E)\frac{1+e^{-E/(k_BT)}}{1-e^{-E/(k_BT)}}\frac{dE}{E}\right], \tag{5}$$

where m is the mass of the resonant nucleus, $n(E,T)$ is the Bose-Einstein distribution function, and E_R is the recoil energy. Additionally, the mean-square atomic displacement parameter (ADP), $\langle u^2\rangle$, of the Mössbauer atom can be calculated using the relation $\langle u^2\rangle = -\ln(f_{\rm LM})/k_{\rm in}^2$. Considering that $\overline{F}$ and $E_{\rm int}$ strongly depend on the spectral weight at high

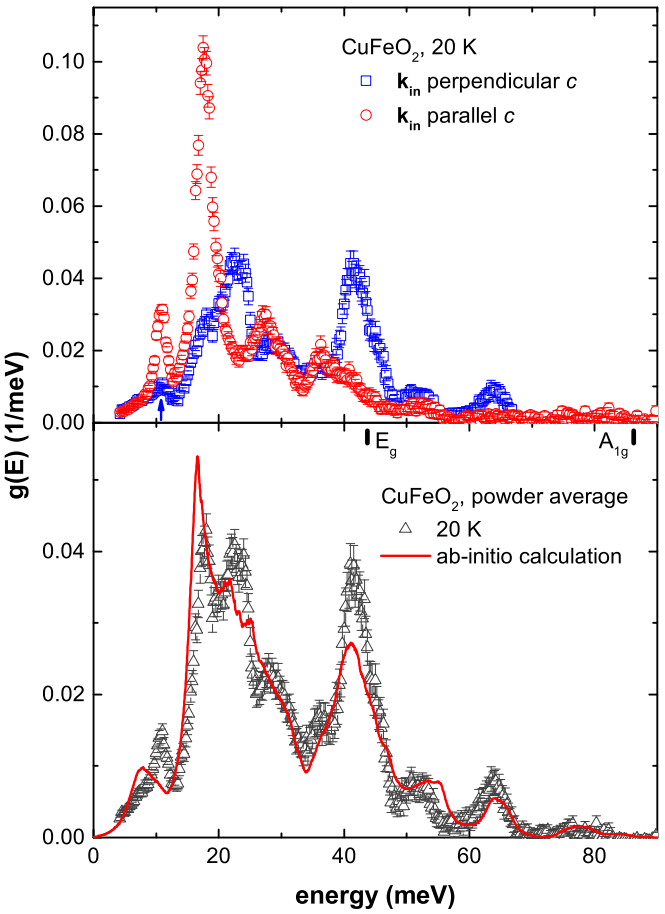

FIG. 5. (Color online) Fe-specific DPS (top) as determined for different orientations of the crystal with respect to the wave vector of the incident beam. Only 20 K results are shown, as no temperature-dependent change of experimental NIS spectra or derived DPS can be detected. The blue arrow indicates that there is a slight admixture of phonons polarized along c in the perpendicular setting due to the nonperfect sample orientation. Above 70 meV, the ($\mathbf{k_{in}} \perp c$) DPS does not exhibit any significant phonon contribution. (Bottom) Calculated powder average of the Fe-specific DPS in $CuFeO_2$ in comparison with an *ab initio* calculation (see Fig. 8 for the calculated, total DPS in $CuFeO_2$).

phonon energies, it is not surprising that the mean force constant and the internal energy are significantly larger for vibrations polarized perpendicular c, whereas the anisotropy of the DPS is not reflected in the ADPs, the Lamb-Mössbauer factors or the vibrational entropy (see Table I). The low-energy limit of the DPS divided by energy squared, the Debye level $L_D = \lim_{E\to 0}[g(E)/E^2]$, can be used to calculate the average phonon group velocity [53] according to

$$v_s^{\mathrm{NIS}} = \sqrt[3]{\frac{m}{\overline{m}}\frac{1}{2\pi^2 n\hbar^3 L_D}}, \tag{6}$$

where m is the resonant mass (^{57}Fe in the present case), $\overline{m}$ is the average atomic mass in the unit cell, and n is the atomic density. The reduced DPS, i.e., DPS$/E^2$, derived from the two 20 K measurements and for the powder averaged case, are shown in Fig. 6. However, none of the reduced DPS exhibits a well defined, constant limit in the low-energy region. In order to estimate the average group velocity in each case anyway, an upper limit, $v_s^{\mathrm{NIS,UL}}$, was calculated by identifying L_D with $g(E)/E^2$ at $E = 4.25$ meV, and a lower limit, $v_s^{\mathrm{NIS,UL}}$, was obtained by the extrapolation of L_D using a linear fit of $g(E)/E^2$ in the energy interval from 4 to 8 meV. Both approaches are represented in Fig. 6 by the horizontal lines and by the decreasing linear slope, respectively. The calculated average group velocities are also summarized in Table I. In general, the calculated ranges of the average phonon group velocity superimpose each other and, thus, there is no direct indication for any acoustic anisotropy for phonons polarized parallel and perpendicular c.

TABLE I. The average phonon group velocity v_s, the mean force constant $\overline{F}$, the vibrational entropy S_{vib}, the internal energy E_{int}, the Lamb-Mössbauer factor f_{LM}, and the mean-square atomic displacement parameter $\langle u^2\rangle$ calculated for Fe-specific vibrations polarized along the c axis ($k_{\mathrm{in}} \parallel c$), within the ab plane ($k_{\mathrm{in}} \perp c$) and for the calculated powder average. DPS derived from 20 K measurements were used for the calculation. The average speed of sound based on ultrasonic velocity measurements, v_s^{US}, was calculated from data in Ref. [22].

	$k_{\mathrm{in}} \parallel c$	$k_{\mathrm{in}} \perp c$	Powder average
E_{int} (meV)	37(3)	47(4)	44(2)
f_{LM}	0.90(2)	0.92(2)	0.91(1)
$\overline{F}$ (N/m)	170(15)	261 (25)	231(17)
S_{vib} (k_b/atom)	0.018(2)	0.018(3)	0.018(2)
$\langle u^2\rangle$ (100 Å^2)	0.20(4)	0.16(4)	0.17(3)
$v_s^{\mathrm{NIS,LL}}$ (m/s)	2370(50)	2420(50)	2430(50)
$v_s^{\mathrm{NIS,UL}}$ (m/s)	2670(100)	2800(100)	2750(100)
v_s^{US} (m/s)			2110 [22]

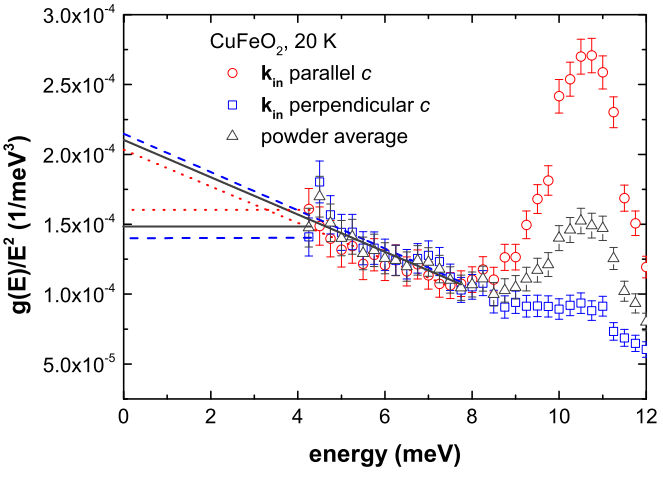

FIG. 6. (Color online) Reduced, Fe partial densities of phonon states in $CuFeO_2$ measured in two different experimental settings at 20 K and in the calculated powder average. The low-energy limit, i.e., the Debye level, was calculated in two different ways (see text for details) and is shown by dotted lines ($k_{\mathrm{in}} \parallel c$), dashed lines ($k_{\mathrm{in}} \perp c$), and solid lines (powder average).

Elastic constants measured using ultrasonic techniques [22] allow for independently estimating the expected average phonon group velocity, v_s^{US}, in $CuFeO_2$. Using the software MINUTI [54], v_s^{US} was calculated to be 2110 m/s in the Voigt-Reuss-Hill approximation [55] (see also Table I) and corresponds to a Debye level $L_D \approx 3.3\times10^{-4}$, which exceeds the present results by a factor of about 2. This discrepancy thus cannot be attributed solely to experimental or data analysis issues and, instead, might be interpreted to reflect a strong deviation from Debye-like behavior at low energies in $CuFeO_2$. In particular, magnetoelastic coupling can reduce the slope of the acoustic phonon dispersion branches [56] in the energy region well below 3 meV, which, in turn, would result in an increased "Debye level" at low phonon energies. Thus, the considerable underestimation of the average phonon group velocity by means of NIS may point towards a significant spin-phonon coupling, which was already shown to be necessary in order to model the magnetic behavior [3,21] of $CuFeO_2$. In addition to ultrasound-based investigations [22,23], the present results concerning the low-energy region indicate that magnetoelastic coupling persists in the paramagnetic phase of $CuFeO_2$ as well.

C. *Ab initio* lattice dynamics in $CuFeO_2$

Calculated phonon dispersions along principal directions in the Brillouin zone of $CuFeO_2$ exhibit three major bands (see Figs. 7 and 8). High-frequency oxygen vibrations form a relatively narrow band which contains some admixture of copper vibrations (see also the calculated partial and total densities of phonon states in Fig. 8). This particular band is separated from other vibrations by an energy gap. Below about 75 meV or 600 cm^{-1} oxygen, iron- and copper-specific modes overlap, whereby oxygen dominates at higher energies and metal-ion-specific modes mostly contribute below 40 meV. Available Raman scattering data [51] is also in rather good

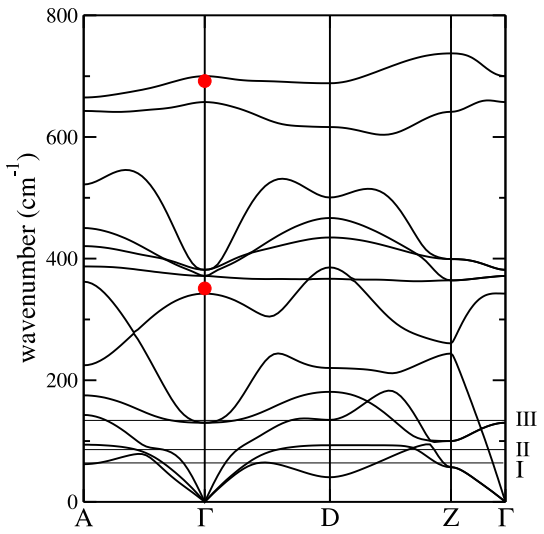

FIG. 7. (Color online) Phonon spectrum of $CuFeO_2$. Solid dots indicate positions of Raman active modes [51]. Labels I, II, and III and corresponding horizontal lines indicate the position of low-energy peaks observed in the DPS (see Fig. 8).

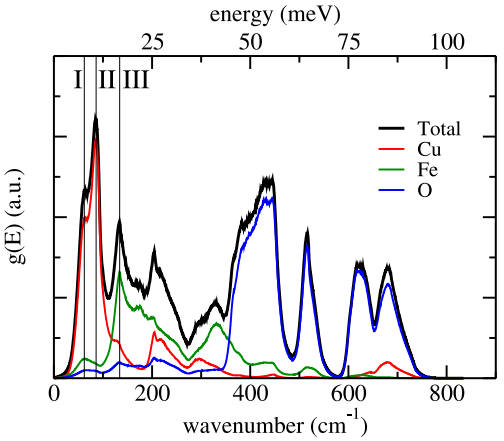

FIG. 8. (Color online) Total and partial DPS in $CuFeO_2$. The labels I, II, and III indicate peak positions in the low-energy range (see text and Fig. 7 for further details).

agreement with calculated modes on the zone center (see Figs. 7 and 8). In general, the calculated phonon spectrum closely resembles [57] the theoretical one of delafossite type $CuGaO_2$, which is not unexpected considering the rather close atomic masses and lattice constants.

Although the overall agreement between the experimentally obtained Fe-specific DPS and the calculated one is rather good, some discrepancies, particularly at low energies, are obvious (see Fig. 5). Considering the calculated DPS, the first Fe-specific mode (labeled I), which originates from acoustic vibrations at the Brillouin zone boundaries in points A, D, and Z, as well on the maximum of the transversal acoustic branch in direction Γ-D (within the range of 10 cm^{-1} used for smearing), is detected at higher energies experimentally. Notably, Cu exhibits a significant spectral contribution at this particular frequency/energy and contributes even more to mode II, which shows a dispersion plateau in the vicinity of the D point (see Fig. 7). Considering that the energy/frequency of mode II fits to the energy/frequency of the first experimental singularity, one might speculate about antisite defects involving Cu and Fe. However, any attempt to model the Fe-specific experimental DPS using a superposition of calculated Cu- and Fe-specific DPS worsens the agreement between experimental and theoretical DPS above 20 meV as Cu-specific vibrations are rather confined at lower energies. On the other hand, mode III, which originates from optical vibrations in the Γ point with some admixture of longitudinal acoustic phonons from points A and D, is clearly dominated by Fe-specific vibrations and matches the experimental data quite well, which substantiates the general validity of the calculations.

It is also interesting to note that calculated phonon group velocities of different acoustic modes are also well above v_s^{US}, although they certainly do not violate the lower limit $v_s^{NIS,LL}$ as determined using NIS (see Table I): In the Γ-A direction, the two transversal acoustic (TA) modes propagate with 2400 and 3400 m/s, whereas the longitudinal mode (LA) propagates with 6415 m/s. In the direction of the c axis (i.e., Γ-Z) two TA modes are doubly degenerated with 2420 m/s and the LA mode reaches 9540 m/s, which is the highest group velocity calculated. The two latter observations, i.e., the

slight underestimation of the energy of the first Fe-specific van Hove singularity as well as the discrepancy between v_s^{US} and calculated phonon group velocities, might indicate the presence of magnetoelastic coupling not appropriately taken into account by the present calculations. In this way, the first van Hove singularity could be pushed to slightly higher energies and the slope of the dispersion at very low, i.e., ultrasonic, energies could be decreased, leading to actually smaller average phonon group velocities.

IV. CONCLUSIONS

Delafossite $CuFeO_2$ was investigated using nuclear resonance scattering by the ^{57}Fe Mössbauer resonance within the temperature interval from 8.5 K to 20 K. Using a ^{57}Fe-enriched single crystal the magnetic structure was indirectly probed by NFS via hyperfine interactions and the vibrational anisotropy was investigated using NIS and compared to *ab initio* calculations.

With respect to hyperfine interactions and magnetism in $CuFeO_2$, the collinear spin structure below T_{N2} could be confirmed and the critical behavior of the average hyperfine field below T_{N1} supports a three-dimensional model of magnetism. Moreover, the observed NFS pattern for $T_{N2} \leqslant T \leqslant T_{N1}$ is incompatible with the assumption of a sinusoidal distribution of spins along c. Instead, the data can be modeled using a phenomenological approach yielding an inhomogeneous distribution of spins with respect to parallelism and antiparallelism along c.

Concerning lattice dynamics, $CuFeO_2$ is characterized by a pronounced vibrational anisotropy with respect to phonon polarization. Lattice vibrations polarized along c are optically softer than their counterparts polarized in the ab plane. This manifests in significant differences between the corresponding force constants and internal energies. The overestimation of the average group velocity by NIS indicates that low-energy phonons in $CuFeO_2$ strongly deviate from a classical Debye-like behavior, which may be due to significant spin-phonon coupling effects at low phonon energies. *Ab initio* calculations of the phonon spectrum in $CuFeO_2$ further substantiate this interpretation as both the first Fe-specific van Hove singularity and the phonon group velocities are incorrectly modeled. However, the overall agreement between experimental and theoretical Fe-specific DPS is good.

From the methodological perspective, the reported results clearly demonstrate the possibilities to reconstruct the total DPS from its projected constituents and to use known magnetic phases as an internal temperature standard. Because $CuFeO_2$ is also considered a potential low-cost thermoelectric material, the vibrational anisotropy suggests that single-crystal material might be worth investigating in the future considering, e.g., the directional dependence [58] of thermoelectric properties of SnSe.

ACKNOWLEDGMENTS

Portions of this research were carried out at the light source PETRA III at DESY, a member of the Helmholtz Association (HGF). We would like to thank Dr. K. Schlage for assistance in using beamline P01. R.P.H. and K.Z.R. acknowledge support from the Helmholtz Association within the Young Investigators Group Programme for Grants No. VH-NG-407 and No. VH-NG-409, respectively. We gratefully acknowledge support by the Jülich Supercomputing Centre and JARA-HPC from RWTH Aachen University under Project No. jara0081. We would also like to thank Dr. C. Strohm for valuable advice. Partly, this research was supported by the German Research Society (DFG) in the framework of Priority Program No. SPP 1386. A.N. acknowledges the use of crystal growth facility in the group of Prof. Thom Plastra at Zernike Institute, RuG.

[1] O. A. Petrenko, G. Balakrishnan, M. R. Lees, D. M. Paul, and A. Hoser, Phys. Rev. B **62**, 8983 (2000).
[2] T. T. A. Lummen, C. Strohm, H. Rakoto, A. A. Nugroho, and P. H. M. van Loosdrecht, Phys. Rev. B **80**, 012406 (2009).
[3] T. T. A. Lummen, C. Strohm, H. Rakoto, and P. H. M. van Loosdrecht, Phys. Rev. B **81**, 224420 (2010).
[4] C. Strohm, T. T. A. Lummen, I. P. Handayani, T. Roth, C. Detlefs, P. J. E. M. van der Linden, and P. H. M. van Loosdrecht, Phys. Rev. B **88**, 060408(R) (2013).
[5] H. Takahashi, Y. Motegi, R. Tsuchigane, and M. Hasegawa, J. Magn. Magn. Mater. **272–276**, 216 (2004).
[6] N. Terada, D. D. Khalyavin, P. Manuel, T. Osakabe, P. G. Radaelli, and H. Kitazawa, Phys. Rev. B **89**, 220403 (2014).
[7] T. Kimura, J. C. Lashley, and A. P. Ramirez, Phys. Rev. B **73**, 220401 (2006).
[8] C. Zhong, H. Cao, J. Fang, X. Jiang, X. Ji, and Z. Dong, Appl. Phys. Lett. **97**, 094103 (2010).
[9] Y. Tanaka, N. Terada, T. Nakajima, M. Taguchi, T. Kojima, Y. Takata, S. Mitsuda, M. Oura, Y. Senba, H. Ohashi, and S. Shin, Phys. Rev. Lett. **109**, 127205 (2012).
[10] T. Okuda, N. Jufuku, S. Hidaka, and N. Terada, Phys. Rev. B **72**, 144403 (2005).
[11] K. Hayashi, T. Nozaki, and T. Kajitani, Jpn. J. Appl. Phys. **46**, 5226 (2007).
[12] R. D. Shannon, C. T. Prewitt, and D. B. Rogers, Inorg. Chem. **10**, 719 (1971).
[13] N. Terada, S. Mitsuda, H. Ohsumi, and K. Tajima, J. Phys. Soc. Jpn. **75**, 023602 (2006).
[14] F. Ye, Y. Ren, Q. Huang, J. A. Fernandez-Baca, P. Dai, J. W. Lynn, and T. Kimura, Phys. Rev. B **73**, 220404 (2006).
[15] S. Mitsuda, N. Kasahara, T. Uno, and M. Mase, J. Phys. Soc. Jpn. **67**, 4026 (1998).
[16] M. Mekata, N. Yaguchi, T. Takagi, S. T, S. Mitsuda, H. Yoshizawa, N. Hosoito, and T. Shinjo, J. Phys. Soc. Jpn. **62**, 4474 (1993).
[17] S. Mitsuda, H. Yoshizawa, N. Yaguchi, and M. Mekata, J. Phys. Soc. Jpn. **60**, 1885 (1991).
[18] N. Terada, Y. Tanaka, Y. Tabata, K. Katsumata, A. Kikkawa, and S. Mitsuda, J. Phys. Soc. Jpn. **75**, 113702 (2006).
[19] N. Terada, Y. Tanaka, Y. Tabata, K. Katsumata, A. Kikkawa, and S. Mitsuda, J. Phys. Soc. Jpn. **76**, 068001 (2007).

[20] N. Terada, Y. Narumi, Y. Sawai, K. Katsumata, U. Staub, Y. Tanaka, A. Kikkawa, T. Fukui, K. Kindo, T. Yamamoto, R. Kanmuri, M. Hagiwara, H. Toyokawa, T. Ishikawa, and H. Kitamura, Phys. Rev. B **75**, 224411 (2007).

[21] F. Wang and A. Vishwanath, Phys. Rev. Lett. **100**, 077201 (2008).

[22] G. Quirion, M. J. Tagore, M. L. Plumer, and O. A. Petrenko, Phys. Rev. B **77**, 094111 (2008).

[23] G. Quirion, M. J. Tagore, M. L. Plumer, and O. A. Petrenko, J. Phys.: Conf. Ser. **145**, 012070 (2009).

[24] R. Röhlsberger, *Nuclear Condensed Matter Physics with Synchrotron Radiation* (Springer-Verlag, Berlin, 2004).

[25] H.-C. Wille, H. Franz, R. Rhlsberger, W. A. Caliebe, and F.-U. Dill, J. Phys.: Conf. Ser. **217**, 012008 (2010).

[26] In the meantime, the energy resolution of P01 could be improved to about 0.9 meV for the ^{57}Fe resonance.

[27] V. G. Kohn and A. I. Chumakov, Hyperfine Interact. **125**, 205 (2000).

[28] Y. V. Shvyd'ko, Phys. Rev. B. **59**, 9132 (1999).

[29] T.-R. Zhao, M. Hasegawa, and H. Takei, J. Cryst. Growth **166**, 408 (1996).

[30] V. G. Kohn, A. I. Chumakov, and R. Rüffer, Phys. Rev. B **58**, 8437 (1998).

[31] Thus, vibrational isotropy within the hexagonal *ab* plane is assumed below the first structural transition temperature, whereas it is given for $R\bar{3}m$.

[32] G. Kresse and J. Hafner, Phys. Rev. B **47**, 558 (1993).

[33] G. Kresse and J. Furthmüller, Phys. Rev. B **54**, 11169 (1996).

[34] G. Kresse and D. Joubert, Phys. Rev. B **59**, 1758 (1999).

[35] P. E. Blöchl, Phys. Rev. B **50**, 17953 (1994).

[36] J. P. Perdew and A. Zunger, Phys. Rev. B **23**, 5048 (1981).

[37] S. L. Dudarev, G. A. Botton, S. Y. Savrasov, C. J. Humphreys, and A. P. Sutton, Phys. Rev. B **57**, 1505 (1998).

[38] H. J. Monkhorst and J. D. Pack, Phys. Rev. B **13**, 5188 (1976).

[39] A. M. Sukeshini, H. Kobayashi, M. Tabuchi, and H. Kageyama, Solid State Ionics **128**, 33 (2000).

[40] K. Kunc and R. M. Martin, Phys. Rev. Lett. **48**, 406 (1982).

[41] D. Alfè, Comp. Phys. Commun. **180**, 2622 (2009).

[42] S. Nakamura, A. Fuwa, and N. Terada, J. Phys. Soc. Jpn. **83**, 044701 (2014).

[43] The quadrupole splitting $e^2QV_{zz}/2$, where e is the electron charge, Q is the nuclear quadrupole moment, and V_{zz} is the principle component of the EFG, is given either in units of the natural line width Γ_0 of the Mossbauer transition of ^{57}Fe or in units of mm/s to facilitate direct comparability with conventional Mossbauer spectroscopy.

[44] In particular, this includes different values and different directions of hyperfine fields and/or electric field gradients.

[45] G. Le Caër and S. M. Dubiel, J. Magn. Magn. Mater. **92**, 251 (1990).

[46] D. H. Choi, I.-B. Shim, and C. S. Kim, J. Magn. Magn. Mater. **320**, e575 (2008).

[47] H. Keller and I. M. Savic, Phys. Rev. B **28**, 2638 (1983).

[48] J. C. Le Guillou and J. Zinn-Justin, Phys. Rev. Lett. **39**, 95 (1977).

[49] O. A. Petrenko, M. R. Lees, G. Balakrishnan, S. de Brion, and G. Chouteau, J. Phys.: Condens. Matter **17**, 2741 (2005).

[50] M. Malvestuto, F. Bondino, E. Magnano, T. T. A. Lummen, P. H. M. van Loosdrecht, and F. Parmigiani, Phys. Rev. B **83**, 134422 (2011).

[51] V. S. Rusakov, I. A. Presnyakov, A. V. Sobolev, A. M. Gapochka, M. E. Matsnev, and A. A. Belik, JETP Lett. **98**, 544 (2014).

[52] J. Pellicer-Porres, A. Segura, E. Martínez, A. M. Saitta, A. Polian, J. C. Chervin, and B. Canny, Phys. Rev. B **72**, 064301 (2005).

[53] M. Y. Hu, W. Sturhahn, T. S. Toellner, P. D. Mannheim, D. E. Brown, J. Zhao, and E. E. Alp, Phys. Rev. B **67**, 094304 (2003).

[54] W. Sturhahn, MINUTI version 1.1.1, (2015), www.nrixs.com.

[55] R. Hill, Proc. Phys. Soc. A **65**, 349 (1952).

[56] W. Wettling, W. Jantz, and H. Dtsch, Appl. Phys. **23**, 195 (1980).

[57] S. Kumar and H. Gupta, Comput. Theor. Chem. **977**, 78 (2011).

[58] L.-D. Zhao, S.-H. Lo, Y. Zhang, H. Sun, G. Tan, C. Uher, C. Wolverton, V. P. Dravid, and M. G. Kanatzidis, Nature (London) **508**, 373 (2014).